Nuclear matter radii of neutron-deficient Kr isotopes

T. Yamaguchi,[1] T. Suzuki,[1] T. Ohnishi,[2] F. Becker,[3] M. Fukuda,[4] H. Geissel,[3] M. Hosoi,[1] R. Janik,[5] K. Kimura,[6] T. Kuboki,[1] S. Mandel,[3] M. Matsuo,[7] G. Münzenberg,[3] S. Nakajima,[1] T. Ohtsubo,[7] A. Ozawa,[8] A. Prochazka,[5] M. Shindo,[3,9] B. Sitár,[5] P. Strmeň,[5] T. Suda,[2] K. Sümmerer,[3] K. Sugawara,[1] I. Szarka,[5] M. Takechi,[4] A. Takisawa,[7] K. Tanaka,[2] and M. Yamagami[2]

[1]*Department of Physics, Saitama University, Saitama 338-8570, Japan*
[2]*The Institute for Physical and Chemical Research (RIKEN), Saitama 351-0198, Japan*
[3]*Gesellschaft für Schwerionenforschung (GSI), D-64291 Darmstadt, Germany*
[4]*Department of Physics, Osaka University, Osaka 560-0043, Japan*
[5]*Faculty of Mathematics and Physics, Comenius University, 84215 Bratislava, Slovak Republic*
[6]*Nagasaki Institute of Applied Science, Nagasaki 851-0193, Japan*
[7]*Department of Physics, Niigata University, Niigata 950-2181, Japan*
[8]*Institute of Physics, University of Tsukuba, Ibaraki 305-8571, Japan*
[9]*Department of Physics, The University of Tokyo, Tokyo 113-0033, Japan*

(Received 18 December 2007; published 31 March 2008)

Interaction cross sections (σ_I) of ^{72,76,80}Kr on a C target were measured at the projectile fragment separator FRS at GSI. Effective matter radii of the nuclei were deduced by a Glauber model analysis so as to reproduce the experimental σ_I. An increase of matter radii toward the proton drip-line is observed. We compare the extracted radii to theoretical predictions, which are based on Skyrme-Hartree-Fock-Bogoliubov (SHFB) and on relativistic mean field (RMF) approaches. The enhancement of the matter radius observed in ^{72}Kr is discussed.

DOI: 10.1103/PhysRevC.77.034315 PACS number(s): 21.10.Gv, 25.70.Mn, 27.50.+e

I. INTRODUCTION

Precision measurements of the interaction cross sections (σ_I) at relativistic energies ($\sim 1A$ GeV) allow us to derive nuclear matter radii [1]. Since nuclear matter radii are directly related to the density distributions, measurements of σ_I are a good tool to search for unusual nuclear structures such as halos and skins. We have performed several experiments and have successfully determined effective rms matter radii ($\tilde{r}_m \equiv \langle r_m^2 \rangle^{1/2}$) of unstable nuclei in the light mass region [2–7]. Such systematic studies have led to the discovery of a new magic number $N = 16$ in light neutron-rich nuclei [8] and evidence for proton skins in proton-rich Ar isotopes [7]. So far, $\tilde{r}_m$ measured via σ_I have been determined up to the mass $A \sim 40$ region.

Recently, an anomalous behavior of $\tilde{r}_m$ of proton-rich Ga, Ge, As, Se, and Br nuclei was reported by measuring the reaction cross sections (σ_R) at intermediate beam energies [9,10]. The authors of Refs. [9,10] claim to have observed a decrease of $\tilde{r}_m$ with increasing neutron number for all isotopic series they have studied. The nuclear structure of the neutron-deficient Kr isotopes close to the $N = Z$ line, including the self-conjugate nucleus ^{72}Kr, attracts particular interest. These isotopes are located in the middle of the fp shell, around the shell gaps according to the deformed shell model, where competing prolate-spherical or oblate-spherical shape transitions have been predicted for many years. Adding or removing a few nucleons to or from a nucleus can change its nuclear shape dramatically. Recent Coulomb excitation and γ spectroscopy experiments [11–16] have indicated large deformations in this region, and even evidence of shape coexistence for ^{72,74,76}Kr.

Gross properties of krypton isotopes such as masses [17,18], half-lives [19], and charge radii, as well as spins and moments [20] have been studied extensively. A measurement of matter radii would provide additional macroscopic information that allows us to determine the ground-state properties of these nuclei. In this paper we present results of $\tilde{r}_m$ of the neutron-deficient isotopes ^{72,76,80}Kr studied via their σ_I measured at relativistic energies, and discuss the systematics of $\tilde{r}_m$ in this region.

II. EXPERIMENT

The experiment was performed at the fragment separator FRS at GSI, Darmstadt [21]. A primary beam of ^{80}Kr accelerated by the SIS synchrotron to an energy of $1.05A$ GeV impinged on a Be target at the entrance of FRS to produce secondary beams of ^{72,76}Kr through projectile fragmentation. A total of three different settings of the FRS were used to select ^{72,76,80}Kr as the central beams. A 2512 mg/cm^2 thick Be target was used for ^{72}Kr, 1032 mg/cm^2 thick for ^{76}Kr, and no production target for ^{80}Kr. A typical primary-beam intensity of 5×10^8 particles per spill was used to produce ^{72}Kr.

The experimental setup is sketched in Fig. 1. Since the details of the measurements have already been given in Ref. [22], we restrict ourselves here to a short summary of the relevant techniques. At the first focus (F1), we placed a scintillation counter to obtain the start signal for a time-of-flight (TOF) measurement. It also served as an active slit for momentum definition ($\Delta p/p = \pm 0.2\%$). At the momentum-dispersive intermediate focus (F2) of FRS (dispersion: 7 cm/%), we installed another plastic scintillation counter to obtain the TOF stop signal (flight path length $l = 17.8$ m). The TOF resolution of 33 ps (FWHM) obtained for the primary beam was sufficient to unambiguously identify the mass numbers A of the particles of interest. It should be noted here that the lifetimes of isomeric states, such as $\tau = 4.53(59)$ ps for the 2_1^+ state of ^{72}Kr [14] and $\tau = 41.2(6)$ ps for the 2_1^+ state of ^{76}Kr [16] are safely shorter than the flight time of $\sim$140 ns between the production target

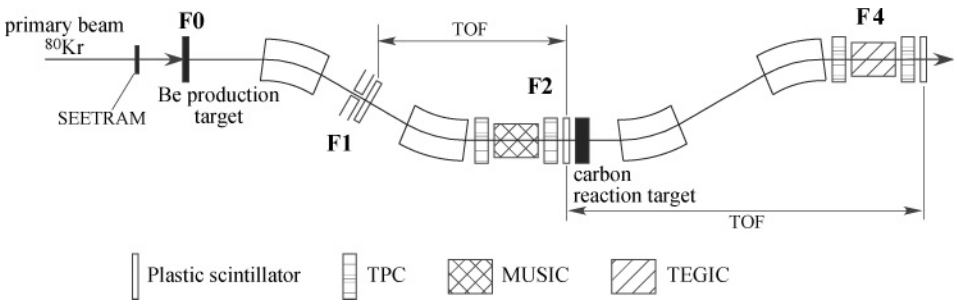

FIG. 1. Experimental setup at the fragment separator FRS.

(F0) and the reaction target (F2). The question of a possible admixture of the 0_2^+ shape isomer in ^{72}Kr will be discussed below in Sec. III.

The fragment nuclear charge number Z was determined by an energy-loss (ΔE) measurement with the ionization chamber, MUSIC [23]. A ΔE resolution of 0.6% in σ was obtained, corresponding to a Z-resolving power of $\Delta Z = 0.33$ (FWHM). Additionally, we positioned two time-projection chambers (TPC) [24] at F2 to tune the separator and to monitor the secondary-beam emittance. The position information at the foci F1 and F2 together with the magnetic field in the second dipole magnet gave $B\rho$ of the fragments. Note that the charge state q of the ions can be assumed at this beam energy to be identical to their nuclear charge numbers Z with probability larger than 99.9%, according to GLOBAL [25] calculations. We could thus calculate A/Z and Z, providing event-by-event particle identification of the secondary beams impinging at F2.

Secondary beams of ^{72,76}Kr were delivered to a 2.30 g/cm^2 thick carbon reaction target located at F2. The nonuniformity in the thickness of this target was negligible. Particle identification in the second half of FRS, F2–F4, was performed in a manner similar to that used in the first part, F1–F2. To this end, a setup at F4, consisting of two TPCs, an ionization chamber (TEGIC [26]), and a plastic scintillation counter, allowed us to determine $B\rho$, TOF, and ΔE.

The principle of the interaction cross section measurements was based on the transmission method. The first and the second half of FRS were used as a spectrometer to identify incoming and outgoing particles, respectively. $\sigma_{\rm I}$ is derived from $\sigma_{\rm I} = -\frac{1}{t} ln(\frac{\Gamma}{\Gamma_0})$, where Γ is the ratio of the number of noninteracting outgoing particles relative to the incoming particles. Γ_0 is the same ratio for an empty-target measurement to correct for nuclear reactions in the detectors, and t denotes the number of target nuclei per unit area. It is essential for the transmission method to count accurately all noninteracting particles downstream of the reaction target. A small-emittance cut was applied for the incident beams based on the position information from the TPCs at F2 in order to ensure full transmission in the second half of FRS. The $\sigma_{\rm I}$ determined in this manner are listed in Table I.

III. DATA ANALYSIS

Before obtaining the rms matter radii from the measured $\sigma_{\rm I}$, we estimated the contribution of electromagnetic dissociation (EMD) of the Kr projectiles, $\sigma_{\rm EMD}$. This cross section can be assumed to be small in view of the small atomic number of the C target; this is verified in a simple calculation shown below. In addition, we paid attention to the admixture of isomeric states in ^{72,76}Kr.

A. Estimate of the electromagnetic-dissociation contribution

EMD can be assumed to occur via virtual-photon excitation of the giant dipole resonance, followed by particle decay. At the high energy of our experiment, single-step $E1$ excitation is the dominant process. Its strength can be estimated by using the "$E1$ sum rule" [27] of $\sigma = 60 \times NZ/A$ (mb MeV). The integrated flux of virtual photons around a GDR energy of 19 ($\sim 79 \times (A)^{-1/3}$) $\pm$ 2.6 ($\sim 0.5 \times 90 \times (A)^{-2/3}$) MeV is estimated to be 0.036 MeV^{-1} using the equivalent-photon method [28]. Thus $\sigma_{\rm EMD}$ via this process is estimated to be approximately 38 mb. Significant low-lying $E1$ strength is not expected to occur for the well-bound nuclei of this experiment, therefore an estimate of $\sigma_{\rm EMD}$ using only the GDR strength is sufficient. Since the EMD contribution of $\approx$38 mb quoted above is comparable to or smaller than the errors of the interaction cross sections, we use the $\sigma_{\rm I}$ listed in Table I for further discussion. The uncertainty of 40 mb in $\sigma_{\rm I}$ corresponds to an uncertainty of 0.08 fm in $\tilde{r}_{\rm m}$.

B. Population of isomeric states

In the present setup for $\sigma_{\rm I}$ measurements, the secondary projectile could be produced in an isomeric state that lives long enough to be transmitted to the secondary target at F2. We have therefore checked for this possibility, with the exception of ^{80}Kr. It is known that there is a low-lying metastable isomeric 0_2^+ state in ^{76}Kr [29]. This state is located 346 keV above the 2_1^+ state. A $0_2^+ \rightarrow 2_1^+$ $E2$ transition occurs, which is known to be dominant by a factor of 490(19) over the $E0$ transition. Other excited states up to about 4.5 MeV have shorter half-lives than the 0_2^+ state. The mean lifetime of the 0_2^+ state is 61(9) ps [29] in the rest frame and 124(18) ps in the laboratory

TABLE I. Interaction cross sections ($\sigma_{\rm I}$) in millibarns for Kr isotopes with mass number A and their nuclear effective rms matter radii ($\tilde{r}_{\rm m}$) in fm.

A	$\sigma_{\rm I}$	$\tilde{r}_{\rm m}$
80	2034(21)	4.029(42)
76	2002(19)	4.002(41)
72	2195(138)	4.43(27)

frame, which is safely much shorter than the flight time of ∼140 ns between the production target (F0) and the reaction target (F2).

A 0_2^+ state occurs also in ^{72}Kr [12]. Here, the situation should be considered more carefully, since only the $E0$ transition $0_2^+ \rightarrow 0_{g.s.}^+$ is energetically allowed. The decay by internal conversion is to first order blocked for fully stripped ions. The mean lifetimes of the 0_2^+ state in the rest frame and that in the laboratory frame are 38(3) ns [12] and 75(6) ns, respectively. Thus a produced isomeric state may reach the reaction target. At GANIL, the isomeric ratio $P(0_2^+)/P(0_{g.s.}^+)$ of the 0_2^+ shape isomer in ^{72}Kr produced by projectile fragmentation of ^{78}Kr on a ^{9}Be target was found to be 5.5(12)(7)% at 73A MeV [30]. Other systematics of isomeric ratios can be found in [31], where isomers (^{84}Nb, ^{88}Zr, ^{90}Mo, and so on) produced via the fragmentation of 750A MeV ^{107}Ag on a ^{9}Be target were studied. The population ranges are 9(1)%–42(11)% for $J^\pi = 5^- \sim 14^+$.

Since the energy dependence of the production mechanism is unclear, we estimated the isomeric ratio using a fragmentation model based on geometrical abrasion [32]. Under the present experimental conditions, the excitation energy of the prefragments is assumed to be around 27 MeV and the average number of evaporated nucleons to be two. As one can see from Fig. 2, this model predicts the isomeric ratio for $J = 0$ to reach 30%. The difference in the charge radius between the ground state and the isomeric state can be found to be 0.005 fm for ^{79}Kr [20], which amounts to only 0.1%. We arbitrarily assume that the radius of $0_{g.s.}^+$ differs from that of 0_2^+ by 10% (∼0.4 fm). Under these assumptions, the contribution of the 0_2^+ state to the measured matter radius is 3%. This is smaller than the uncertainty of 0.27 fm in $\tilde{r}_m$, and therefore, the mixing of the 0_2^+ shape isomer in ^{72}Kr does not affect the results within the present statistical uncertainty.

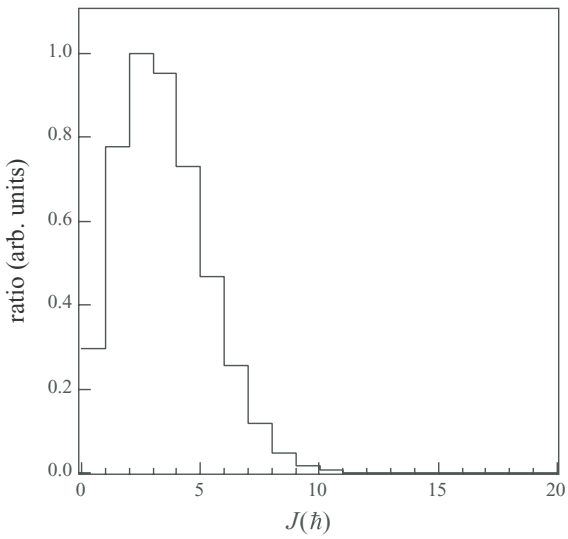

FIG. 2. The angular momentum distribution of ^{72}Kr via fragmentation of ^{80}Kr + ^{9}Be → ^{72}Kr at 1A GeV as calculated in the geometrical-abrasion model [32]. The distribution is normalized to its maximum value.

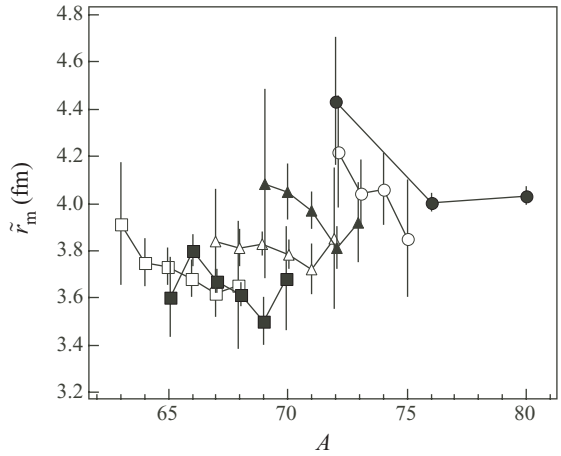

FIG. 3. Effective rms matter radii of Ga (open squares), Ge (filled squares), As (open triangles), Se (filled triangles), Br (open circles) [9], and present results for Kr (filled circles). The lines are to guide to eye.

C. Determination of matter radii

Based on the Glauber model in the optical limit [33], $\tilde{r}_m$ were deduced from measured σ_I. It should be noted that at relativistic beam energies the relation $\sigma_R = \sigma_I + \sigma_{inelastic}$ is well approximated by $\sigma_R \simeq \sigma_I$ [7].

A harmonic-oscillator type density distribution, which reproduces the densities of light nuclei well, was used for the target (^{12}C). For the projectiles (^{72,76,80}Kr), a Fermi type function was employed as the density distribution, $\rho(r) = \frac{\rho_0}{1+\exp(\frac{r-R}{a})}$, where R and a denote the half density radius and the diffuseness parameter, respectively. We fixed the diffuseness parameter to be $a = 0.5$ fm which was obtained experimentally by studying electron scattering from ^{88}Sr [34]. The resulting $\tilde{r}_m$ of ^{72,76,80}Kr are listed in Table I and shown in Fig. 3 together with those of Ga, Ge, As, Se, and Br isotopes measured at GANIL [9,10].

IV. RESULTS AND DISCUSSIONS

A. Variation of the radius with atomic and neutron number

Recently, Lima *et al.* [9,10] have measured σ_R of proton-rich Ga, Ge, As, Se, and Br isotopes at intermediate energies using a telescope of stacked Si detectors surrounded by Ge detectors. It is observed that for all isotopes $\tilde{r}_m$ tends to decrease as the mass number increases, although the experimental uncertainties are relatively large due to the efficiency corrections for the Ge detectors. The present result for the Kr isotopes is consistent with this behavior of $\tilde{r}_m$. To make the systematic behavior of the radii clear, the atomic number (Z) dependence of $\tilde{r}_m$ for $N = 36$ isotones is plotted in Fig. 4. It is clear that the $\tilde{r}_m$ increase monotonically toward the proton-drip line. The solid and dashed lines indicate RMF predictions with the NL3 and TMA parameter set, respectively. The RMF calculation with the NL-SH interaction presented in Ref. [37] reproduces the systematics of the isotope shifts well, while similar calculations agree with one another but

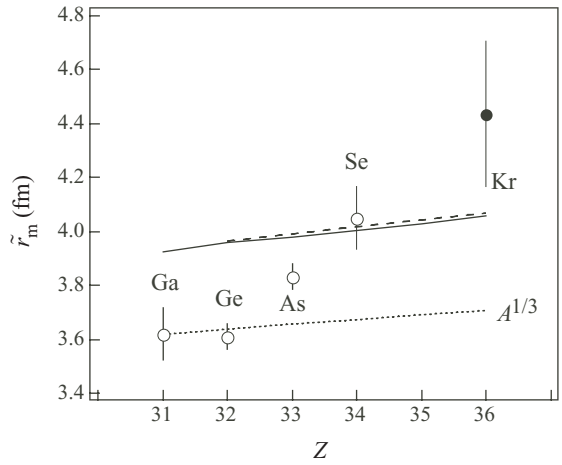

FIG. 4. Atomic number dependence of $\tilde{r}_m$ for $N = 36$ isotones. Data for Ga, Ge, As, and Se shown by open circles were taken from Ref. [9]. The dotted line shows the $A^{1/3}$ dependence of the matter radii normalized to Ga. The solid [35] and dashed [36] lines are theoretical predictions.

fail to reproduce the atomic number dependence of $\tilde{r}_m$. The experimental atomic number dependence is steeper than what is predicted by theory when adding a proton to a nucleus. The $\tilde{r}_m$ increase more strongly with Z than with $A^{1/3}$.

In Fig. 5 we plot the evolution of $\tilde{r}_m$ and rms proton radii ($\tilde{r}_p \equiv \langle r_p^2 \rangle^{1/2}$), which were extracted from charge radii ($\tilde{r}_{ch.} \equiv \langle r_{ch.}^2 \rangle^{1/2}$) [20], using the relation $\langle r_p^2 \rangle = \langle r_{ch.}^2 \rangle - 0.8^2$. The RMF calculation with the NL-SH interaction presented in Ref. [37] reproduces the systematics of the isotope shifts well but once again does not reproduce $\tilde{r}_m$. Recent Dirac-Hartree-Bogoliubov (DHB) calculations [38] also do not show a decrease in $\tilde{r}_m$ with the increase in neutron number for proton-rich isotopes of Ga, Ge, As, Se, and Br, although the

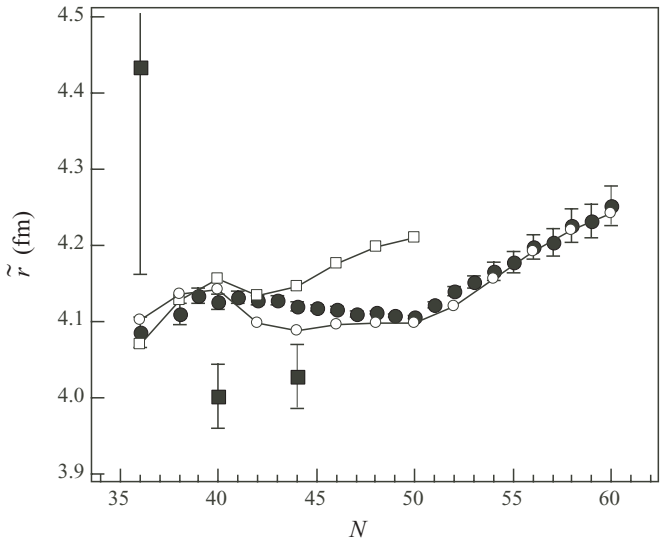

FIG. 5. Neutron number dependence of rms matter and proton radii. Closed symbols indicate the experimental data of $\tilde{r}_m$ (squares) and $\tilde{r}_p$ (circles) from $\tilde{r}_{ch}$ [20]. Corresponding open symbols connected by lines show theoretical predictions [35].

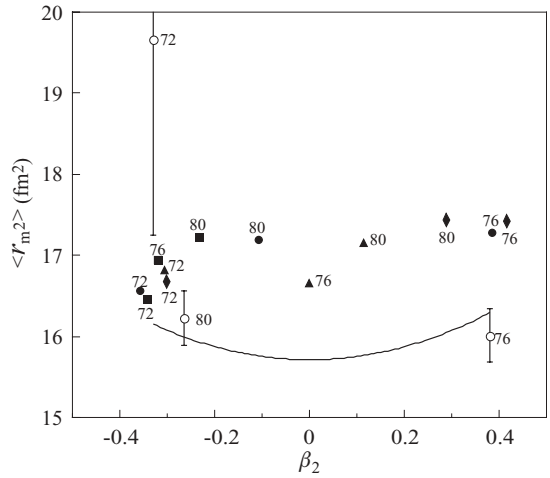

FIG. 6. Two-dimensional plot of β_2 versus $\langle r_m^2 \rangle$ for ^{72,76,80}Kr. Open symbols show the experimental data. The curve indicates the result of the fit to the parabolic form of $\langle r_m^2 \rangle = \langle r_m^{2\ \text{spherical}} \rangle (1 + \frac{5}{4\pi}\beta_2^2)$. The closed symbols indicate theoretical predictions by RMF with NL3 (circles) [35], RMF with TMA (squares) [36], Skyrme-Hartree-Fock-Bogoliubov (SHFB) with SkM* (diamonds), and SHFB with SLy4 (triangles). Details of the SHFB calculation are given in Ref. [43]. The corresponding mass number is indicated at each data point.

DHB calculation describes the total binding energies well. The DHB results show a smooth increase in $\tilde{r}_m$ with both, increasing neutron and increasing proton numbers.

B. Variation of the radius with the deformation

The correlation between the matter radii and deformation for proton-rich Ga, Ge, As, Se, and Br isotopes was studied by the authors of Refs. [9,10]. The excitation energies of the first 2^+ state for even-even nuclei and those of the first excited state with $J = J_{g.s.} + 2$ for odd-even nuclei were compared with observed $\tilde{r}_m$. They reported that no correlation was seen between an increase in deformation and the increase in radial extension with decreasing N for Ga, Ge, As, Se, and Br.

For krypton isotopes theory predicts a change in the shape of the ground state [39] from predominantly oblate in ^{72}Kr to prolate in ^{76}Kr. An oblate ground state ($|\beta_2| = 0.33$) [14] in ^{72}Kr and a prolate ground state ($|\beta_2| = 0.38$) [15] in ^{76}Kr have been observed experimentally. It is known that ^{80}Kr has an oblate ground state deformation ($|\beta_2| = 0.25$) [40].

Figure 6 shows the two-dimensional plot of the β_2 versus $\langle r_m^2 \rangle$. Here we followed the procedure described in Ref. [41], which is based on a "pairing-plus-quadrupole" model [42], where the nuclear shapes are parametrized as rotational ellipsoids with the deformation being limited to the quadrupole contribution. Under this assumption, $\tilde{r}_m$ can be written as the parabolic form of β_2; $\langle r_m^2 \rangle = \langle r_m^{2\ \text{spherical}} \rangle (1 + \frac{5}{4\pi}\beta_2^2)$. If we further assume that the radii of the krypton isotopes are simply described by the above two parameters, β_2 and the spherical part of the nuclear radius ($\tilde{r}_m^{\text{spherical}}$), a deviation from the parabolic curve for ^{72}Kr is seen.

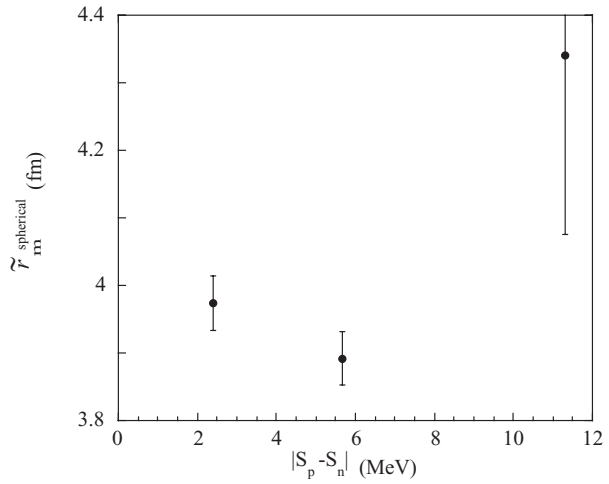

FIG. 7. Two-dimensional plot of the spherical part of nuclear radii versus $|S_p\text{-}S_n|$ for ^{72,76,80}Kr.

In Fig. 6, theoretical predictions are also plotted for comparison. It can be seen that none of the calculations simultaneously reproduce $\langle r_m^2 \rangle$ and β_2. This could be due to a dependence of the shape of the ground state predicted by theory on the effective interactions. The potential-energy curves obtained by these calculations (see, e.g., [36,43]) show two or three local minima close in energy, indicating shape coexistence.

The present work measures σ_I without nuclear orientation, thus in principle the deduced $\tilde{r}_m$ are not sensitive to the nuclear shape. The natural interpretation is that the admixture of oblate deformation increases when going to more neutron-deficient nuclei, which more than compensates for the volume effect of decreasing mass.

As shown in Fig. 3, we observe a similar, relatively large increase of $\tilde{r}_m$ in ^{66}Ge and ^{69}Se but not in ^{67}As. The nucleus ^{66}Ge is inferred to have a collective oblate shape with moderate $\beta_2 \sim -0.23$ and $\gamma \sim -54^\circ$ [44]. The nucleus ^{69}Se is also interpreted to have a substantial oblate deformation $|\beta_2| \sim 0.24$–0.85 [45], while little evidence for oblate collectivity in ^{67}As is reported [46]. Therefore, the increase of $\tilde{r}_m$ toward the proton drip-line may be due to other than the axially-symmetric quadrupole deformation such as triaxial or gamma-soft shapes.

C. Variation of the radius with the separation energy

The main driving force for the formation of skin phenomena is the difference between the proton and neutron Fermi energies. The authors of Ref. [7] evaluated the proton skin thicknesses and discussed their correlations with the separation energy differences (S_p-S_n) for proton-rich Ar isotopes. The situation in Kr seems to be different, however, from our previous observation in the Ar isotopes. The observed feature of decreasing matter radii with increasing N is difficult to explain supposing a larger neutron than proton radius, and therefore, we find no such correlation between the proton skin thickness and S_p-S_n.

In Fig. 7, $\tilde{r}_m^{spherical}$ is plotted against $|S_p\text{-}S_n|$. The observed tendency is somewhat similar to that found in Fig. (8b) of Ref. [3]. This fact can be explained by a model in which only the valence nucleons are responsible for the changes in nuclear radii [3].

V. SUMMARY

In summary, we have measured the interaction cross sections of neutron-deficient ^{72,76,80}Kr isotopes and determined their effective rms matter radii based on a Glauber model analysis in the optical-limit approximation. It was shown that the effective rms matter radii around mass $A \sim 70$ at the proton-rich side increase toward the proton drip-line. The increase of $\tilde{r}_m$ toward the proton drip-line may be due to deformations other than axially-symmetric ones and/or contribution from valence nucleons. Further measurements of σ_R of unstable nuclei for the $A > 40$ region are necessary to establish the evolution of $\tilde{r}_m$ on the proton-rich side.

ACKNOWLEDGMENTS

We would like to thank the members of the FRS group and the SIS staff members for their help and K.-H. Behr, A. Bruenle, K. Burkard, and C. Karagiannis for their technical assistance. We thank Dr. J. Miller at LBNL for carefully reading the manuscript. This work was supported in part by the Japanese Ministry of Education, Science, Sports and Culture by Grant-In-Aid for Scientific Research under Program No. B(2) 16340063 and by VEGA, Slovakia.

[1] I. Tanihata *et al.*, Phys. Lett. **B287**, 307 (1992).
[2] T. Suzuki *et al.*, Phys. Rev. Lett. **75**, 3241 (1995).
[3] L. V. Chulkov *et al.*, Nucl. Phys. **A603**, 219 (1996).
[4] T. Suzuki *et al.*, Nucl. Phys. **A658**, 313 (1999).
[5] L. V. Chulkov *et al.*, Nucl. Phys. **A674**, 330 (2000).
[6] A. Ozawa *et al.*, Nucl. Phys. **A691**, 599 (2001).
[7] A. Ozawa *et al.*, Nucl. Phys. **A709**, 60 (2002).
[8] A. Ozawa, T. Kobayashi, T. Suzuki, K. Yoshida, and I. Tanihata, Phys. Rev. Lett. **84**, 5493 (2000).
[9] G. F. Lima *et al.*, Nucl. Phys. **A735**, 303 (2004).
[10] A. Lépine-Szily *et al.*, Eur. Phys. J. A **25**, 227 (2005).
[11] C. Chandler *et al.*, Phys. Rev. C **56**, R2924 (1997).
[12] E. Bouchez *et al.*, Phys. Rev. Lett. **90**, 082502 (2003).
[13] J. J. Valiente-Dobón *et al.*, Phys. Rev. Lett. **95**, 232501 (2005).
[14] A. Gade *et al.*, Phys. Rev. Lett. **95**, 022502 (2005).
[15] W. Korten *et al.*, Nucl. Phys. **A746**, 90 (2004).
[16] E. Clément *et al.*, Phys. Rev. C **75**, 054313 (2007).
[17] D. Rodríguez *et al.*, Phys. Rev. Lett. **93**, 161104 (2004).
[18] D. Rodríguez *et al.*, Nucl. Phys. **A769**, 1 (2006).
[19] I. Piqueras *et al.*, Eur. Phys. J. A **16**, 313 (2003).
[20] M. Keim *et al.*, Nucl. Phys. **A586**, 219 (1995).
[21] H. Geissel *et al.*, Nucl. Instrum. Methods B **70**, 286 (1992).
[22] T. Yamaguchi *et al.*, Phys. Rev. C **74**, 044608 (2006).
[23] A. Stolz *et al.*, Phys. Rev. C **65**, 064603 (2002).
[24] V. Hlinka *et al.*, Nucl. Instrum. Methods A **419**, 503 (1998).
[25] C. Scheidenberger *et al.* Nucl. Instrum. Methods B **142**, 441 (1998).
[26] K. Kimura *et al.*, Nucl. Instrum. Methods A **538**, 608 (2005).

[27] A. Bohr and B. R. Mottelson, *Nuclear Structure* (World Scientific, Singapore, 1998), Vol. 2, p. 475.
[28] J. D. Jackson, *Classical Electrodynamics* (Wiley, New York, 1975), 2nd ed., p. 719.
[29] A. Giannatiempo *et al*., Phys. Rev. C **72**, 044308 (2005).
[30] E. Bouchez, Ph.D. thesis, Universite Louis Pasteur, Strasbourg, 2003 (unpublished).
[31] C. E. Beer, Ph.D. thesis, University of Surrey, 2006 (unpublished).
[32] M. de Jong, A. V. Ignatyuk, and K.-H. Schmidt, Nucl. Phys. **A613**, 435 (1997).
[33] A. Ozawa, T. Suzuki, and I. Tanihata, Nucl. Phys. **A693**, 32 (2001).
[34] H. de Vries *et al*., At. Data Nucl. Data Tables **36**, 495 (1987).
[35] G. A. Lalazissis, S. Raman, and P. Ring, At. Data Nucl. Data Tables **71**, 1 (1999).
[36] L. Geng, H. Toki, and J. Meng, Prog. Theor. Phys. **113**, 785 (2005); http://www.rcnp.osaka-u.ac.jp/Divisions/np2/Research/Thesis/PhD_Geng.pdf
[37] G. A. Lalazissis and M. M. Sharma, Nucl. Phys. **A586**, 201 (1995).
[38] E. Baldini-Neto, B. V. Carlson, and D. Hirata, J. Phys. G: Nucl. Part. Phys. **32**, 655 (2006).
[39] W. Nazarewicz *et al*., Nucl. Phys. **A435**, 397 (1985).
[40] J. Döring *et al*., Phys. Rev. C **52**, 76 (1995).
[41] G. Fricke *et al*., Phys. Rev. C **45**, 80 (1992).
[42] B. S. Reehal and R. A. Sorensen, Nucl. Phys. **A161**, 385 (1971).
[43] M. Yamagami, K. Matsuyanagi, and M. Matsuo, Nucl. Phys. **A693**, 579 (2001).
[44] E. A. Stefanova *et al*., Phys. Rev. C **67**, 054319 (2003).
[45] S. Skoda *et al*., Nuovo Cimento A **111**, 669 (1998).
[46] D. G. Jenkins *et al*., Phys. Rev. C **64**, 064311 (2001).